

## DARK MATTER SUBHALOS IN THE URSA MINOR DWARF GALAXY

V. LORA<sup>1</sup>, A. JUST<sup>1</sup>, F. J. SÁNCHEZ-SALCEDO<sup>2</sup> AND E. K. GREBEL<sup>1</sup>

*Draft version June 21, 2018*

### ABSTRACT

Through numerical simulations, we study the dissolution timescale of the Ursa Minor cold stellar clump, due to the combination of phase-mixing and gravitational encounters with compact dark substructures in the halo of Ursa Minor. We compare two scenarios; one where the dark halo is made up by a smooth mass distribution of light particles and one where the halo contains 10% of its mass in the form of substructures (subhalos). In a smooth halo, the stellar clump survives for a Hubble time provided that the dark matter halo has a big core. In contrast, when the point-mass dark substructures are added, the clump survives barely for  $\sim 1.5$  Gyr. These results suggest a strong test to the  $\Lambda$ -cold dark matter scenario at dwarf galaxy scale.

*Subject headings:* Methods: numerical – Galaxies: dwarf – Galaxies: kinematics and dynamics – Cosmology: dark matter

### 1. INTRODUCTION

The  $\Lambda$  Cold Dark Matter ( $\Lambda$ CDM) model has been proved to be successful in reproducing structure formation on large scales. In the standard paradigm, a nearly scale invariant power spectrum describes the cosmological primordial density fluctuations. If DM is collisionless, the clustering of substructure is scale-invariant down to the free-streaming scale of the CDM particle (e.g., Hofmann et al. 2001; Green et al. 2005). The properties of the subhalos in Milky Way size galaxies have been studied by Gao et al. (2004), Springel et al. (2008) and Diemand et al. (2008) through collisionless DM simulations. They found that 10% of their mass reside in  $\sim 3 \times 10^4$  subhalos with masses in the range of  $10^4 - 10^8 M_\odot$ , following a CDM subhalo-mass function  $dN/dM \propto M^{-1.9}$ .

At scales of dwarf satellite galaxies, a comparison between the model predictions and observations is limited by our poor understanding of the baryonic processes involved in the formation of galaxies. For instance, supernova feedback and gas heating from cosmic sources can alleviate the inconsistency between the observed number of satellite galaxies in the Milky Way halo and the much higher number of subhalos predicted using  $N$ -body  $\Lambda$ CDM simulations (Moore et al. 1999; Klypin et al. 1999; Benson et al. 2002; Somerville 2002; Ostriker et al. 2003; Font et al. 2011). In this model, many satellites are either too faint to be detected in surveys or dark matter subhalos devoid of a baryonic counterpart (Boylan-Kolchin et al. 2011; Bovill & Ricotti 2011).

Some observational consequences of the existence of substructure within galactic halos have been studied in the literature. Romano-Díaz et al. (2008) suggested that long-lived stellar bars can be triggered by a tide from a massive subhalo. Kannan et al. (2012) explored the idea

that the interaction of dark matter subhalos with the gaseous disks of galaxies may generate density enhancements in the gas. Johnston et al. (2002) studied the distribution of carbon stars in the stream of the Sagittarius (Sgr) dwarf galaxy and found that the Sgr debris is more strongly scattered than would be expected if it would be orbiting in a smooth (and thus non-substructured) DM halo, but that is entirely consistent with perturbations by the Large Magellanic Cloud (LMC) alone. In this line of research, Carlberg (2009) modeled the interaction between streams and halo clumps and concluded that stellar streams older than 3 Gyr cannot survive in the presence of subhalos with the masses and numbers predicted by the  $\Lambda$ CDM model. Nevertheless, the density variations in the star stream detected around the globular cluster Palomar 5 and in the galaxy M31 appear to be in agreement with the existence of DM subhalos (Yoon et al. 2011; Carlberg et al. 2011).

The presence of dark-matter subhalos in dwarf spheroidal galaxies (dSph) might have observable consequences and may shed light on the nature of DM particles. For instance, Jin et al. (2005) and Totani (2010) suggested that compact massive dark objects in the halo of dSph galaxies could resolve some long-standing problems in these systems. On the other hand, Peñarrubia et al. (2010) used analytical and  $N$ -body methods to examine the survival of wide stellar binaries against encounters with dark subhalos orbiting in the DM halos of dwarf galaxies. They found that a large fraction of wide binaries can be wiped out due to tidal encounters with these dark substructures. The observations of large separation binaries would impose a strong test to the putative substructure in halos of dwarf galaxies.

Also Ma et al. (2004) studied the gravitational scattering effects caused by subhalos on the phase-space distribution of DM particles in main halos. Their numerical experiments indicate that the number and the mass density of subhalos could be high enough to flatten the main halo's inner cusp within a few dynamical times.

In this work, we will focus on dSph galaxy Ursa Mi-

vlora@ari.uni-heidelberg.de

<sup>1</sup>Astronomisches Rechen-Institut, Zentrum für Astronomie der Universität Heidelberg, Mönchhofstr. 12-14, 69120 Heidelberg, Germany

<sup>2</sup>Instituto de Astronomía, Universidad Nacional Autónoma de México, AP 70-264, 04510 D.F., México

nor (UMi). UMi has the peculiarity of showing a second stellar density peak (or clump) which is believed to be a cold long-lived structure (Palma et al. 2003). This clump has survived because the underlying gravitational potential in UMi must be close to harmonic, which can be accomplished if the density profile of the dark halo has a large core (Kleyna et al. 2003). In addition, Sánchez-Salcedo & Lora (2007) established stringent constraints on the mass and abundance of compact objects in UMi in order to preserve the integrity of cold small-scale clumps seen in some dSph galaxies. In the present work, our aim is to test whether or not the putative subhalos with a mass spectrum as that found in collisionless CDM is consistent with the stellar clump found in UMi. Our work may shed light on the mechanism responsible for the formation of cores in dwarf galaxies because some of them predict dissolution of dark-matter substructures below a scale of  $\sim 1$  kpc. In fact, the core-making mechanisms proposed so far fall in three broad categories: supernova feedback (e.g., Mo & Mao 2004; Mashchenko et al. 2006; Governato et al. 2010, 2012; Pontzen & Governato 2012; Macciò et al. 2012), dynamical friction from infalling baryonic clumps (El-Zant et al. 2001; Romano-Díaz et al. 2009; Goerdt et al. 2010), or a change in any of the basic properties of dark matter particles [e.g., collisional, annihilating, decaying or warm dark matter] (Spergel & Steinhardt 2000; Kaplinghat, Knox & Turner 2000; Cen 2000; Sánchez-Salcedo 2003; Ávila-Reese et al. 2001). Models in the latter category are expected to help erase dark-matter subhalos in dwarf galaxies, e.g., by mass stripping if dark matter is collisional or by suppression of the power in the mass spectrum at small scales if dark matter is warm, whereas models in the first two categories are expected to preserve them.

This article is organized as follows. In §2 we describe some properties of UMi and its clump. The initial conditions for our  $N$ -body simulations are described in §3. The results of the simulations are shown in §4. Finally, we present our conclusions in §5.

## 2. UMI AND ITS CLUMP

UMi is a dSph galaxy satellite of the Milky Way, located at a Galactocentric distance of  $R_{GC} = 69 \pm 4$  kpc (Grebel et al. 2003). Dynamical studies suggest that UMi has a mass-to-light ratio larger than  $60M_{\odot}/L_{\odot}$  (e.g. Wilkinson et al. 2004). Rescaling the results of Gilmore et al. (2007) and taking a luminosity of  $L_V = 1.1 \times 10^6 L_{\odot}^V$  (Palma et al. 2003), the total mass within 0.6 kpc is  $6.3 \times 10^7 M_{\odot}$ , which results in a mass-to-light ratio  $M/L_V \gtrsim 60M_{\odot}/L_{\odot}$  for UMi. It has to be noted that if we take  $L_V = 3 \times 10^5 L_{\odot}$  (Grebel et al. 2003) then we obtain a  $M/L_V \sim 200M_{\odot}/L_{\odot}$  (Gilmore et al. 2007). Deeper data for dwarf galaxies often reveal a larger angular extent of their stellar component (e. g., Odenkirchen et al. 2001; Kniazev et al. 2009); nevertheless, we adopt the lower luminosity value for UMi. The high value of  $M/L$  in UMi implies that it is one of the most dark matter dominated dSph galaxies in the Local Group.

UMi's stellar King core radius along the semimajor axis is 17.9 arcmin ( $\sim 0.4$  kpc) (Palma et al. 2003). UMi shows a large ellipticity in the shape of the inner isoden-

sity contours of the surface density of stars ( $\epsilon = 0.54$ ) (Palma et al. 2003), but the most remarkable feature in UMi's structure is the second off-centered density peak (Kleyna et al. 1998). One of these two peaks is located on the north-eastern side of the major axis of UMi at a distance of  $\sim 0.4$  kpc from UMi's center. The radial velocity distribution of the stars in UMi is well fitted by two Gaussians, one representing the underlying background ( $8.8 \text{ km s}^{-1}$ ) and the other representing the velocity dispersion of the second peak ( $0.5 \text{ km s}^{-1}$ ). The stars in the vicinity of this peak comprise a kinematically distinct cold subpopulation: a dynamically cold stellar clump. The most appealing interpretation of UMi's clump is that it is a disrupted cluster (Read et al. 2006) that orbits in the plane of the sky, and that has survived in phase-space because the underlying gravitational potential is harmonic (Kleyna et al. 2003). This implies that the dark halo density profile in UMi should have a core (and not a cuspy profile as predicted by the  $\Lambda$ CDM paradigm) and that this core must be large ( $\sim 500$  pc, see Kleyna et al. 2003 and Lora et al. 2009).

The stellar population of the UMi dwarf galaxy is very old with an age of 10–13 Gyr; virtually all the stars were formed 10 Gyr ago, and 90% of them were formed 13 Gyr ago (Carrera et al. 2002; Rocha et al. 2011). This implies that star formation was halted at a redshift of  $z \sim 2$ , probably because supernova explosions were able to remove all the gas. In fact, deep observations have not detected gas in UMi (Young 1999, 2000). Gas replenishment from dying stars and stellar winds is expected to be very small. If the gas returned to the interstellar medium by intermediate- and low-mass dying stars were distributed across the galaxy as the stars are, the central gas density would reach a value of  $\sim 4.4 \times 10^{-3} M_{\odot} \text{ pc}^{-3}$  after 10 Gyr (Carrera et al. 2002). This corresponds to a particle density of  $5 \times 10^{-3} \text{ cm}^{-3}$ , much smaller than the typical lower thresholds for star-forming regions ( $\sim 1000 \text{ cm}^{-3}$ ) (Shu et al. 1987). Since we are interested here in the dynamical evolution of the stellar clump over the last 10 Gyr, once essentially all the gas has been removed, we can discard both gas processes and stellar evolution in our simulations.

## 3. $N$ -BODY: INITIAL CONDITIONS AND THE CODE

### 3.1. The dark matter component of UMi

We performed  $N$ -body simulations of the UMi dSph galaxy, which include a baryonic component (the bulk stellar component and the stellar clump) embedded in a spherical (live) dark matter halo. The dark matter halo density profile selected is defined as

$$\rho(r) = \frac{\rho_0}{(r/r_s)^{\gamma} [1 + (r/r_s)^{\alpha}]^{(\beta - \gamma/\alpha)}}. \quad (1)$$

Here  $\rho_0$  accounts for the central density in the case of  $\gamma = 0$  and  $r_s$  is the scale length. A NFW profile (Navarro et al. 1996) is obtained for  $(\alpha, \beta, \gamma) = (1, 3, 1)$ . We have chosen the values  $(\alpha, \beta, \gamma) = (1, 3, 0)$  in order to have a cored DM mass density profile.

It has been found that cored profiles (and not cuspy profiles) are in better agreement with UMi dynamics (Kleyna et al. 2003; Lora et al. 2009). Some other dSph galaxies in the Local Group such as Fornax, Sculptor, Carina, Leo I and Leo II are

also believed to possess cored dark halos instead of cuspy profiles (Kleyna et al. 2003; Goerdts et al. 2006, 2010; Sánchez-Salcedo et al. 2006; Gilmore et al. 2007; Battaglia et al. 2008; Amorisco et al. 2011; Walker & Peñarrubia 2011; Jardel & Gebhardt 2012; Agnello & Evans 2012). Moreover, it is found from high resolution observations of the rotation curves for DM dominated low surface brightness (LSB) galaxies that DM halos have density profiles compatible with flat central cores (de Blok et al. 2001; Chen et al. 2010).

We explored two different cored halos; a small-core halo with a scale length of 0.91 kpc (which corresponds to a core radius of  $\sim 0.4$  kpc) with a total mass of  $M = 2 \times 10^9 M_\odot$ , and a big-core halo with a scale length of 2.2 kpc (core radius  $\sim 1$  kpc) and a total mass of  $M = 3 \times 10^{10} M_\odot$ . For our halo models we have a mass within a radius of 0.39 kpc (the clump’s orbit) of  $\sim 10^7 M_\odot$  for the small-core halo, and a mass of  $\sim 3 \times 10^7 M_\odot$  for the big-core halo model. This is consistent with the results of Strigari et al. (2007, 2008) who considered dark halos compatible with the observed stellar kinematics of the classical dSph galaxies, including the dwarf galaxy UMi. They found that, for realistic density profiles, the mass interior to 300 pc is  $\sim 10^7 M_\odot$  for all dSph galaxies in the Milky Way halo.

To generate the initial conditions of the dark matter particles of the smooth background distribution, we used the distribution function proposed by Widrow (2000), and the velocity dispersion of the system was taken to be isotropic.

In order to explore the dynamical effects of a clumpy halo, we generated the mass spectrum of substructures in the halo following the power-law mass distribution

$$\frac{dN}{dM} = a_0 \left( \frac{M}{M_0} \right)^{-1.9} \quad (2)$$

(Gao et al. 2004; Springel et al. 2008; Diemand et al. 2008). The values of  $a_0$  and  $M_0$  are fixed once the lower  $M_{min}$  and upper  $M_{max}$  mass limits of the substructure particles and the fraction ( $f$ ) of the halo mass comprised in substructures, are given.

The mass of dark matter particles used in our simulations without subhalos is  $2 \times 10^3 M_\odot$ , which corresponds to our maximal mass resolution for the halo particles. Then it is a natural choice to take  $M_{min} = 10^{3.3} M_\odot$  as the lower mass limit. Adopting the subhalo mass function found in CDM simulations, the subhalos are expected to have masses up to  $M_{max} \lesssim 0.1 M_{vir}$ , where  $M_{vir}$  is the virial mass of the halo (Peñarrubia et al. 2010). Given that the estimated average virial mass of the dSph galaxies is of the order of  $M_{vir} \sim 10^9 M_\odot$  (Peñarrubia et al. 2008; Walker et al. 2009), the upper mass limit could be as large as  $10^8 M_\odot$ . It then becomes reasonable to take the generous upper mass limit as  $M_{max} \simeq 10^7 M_\odot$ .

Equation (2) with  $f$ ,  $M_{min}$  and  $M_{max}$  known, determines the number  $N_{SUB}$  of substructure particles. In order to construct a clumpy DM halo, we choose from the original smooth DM halo, a number  $N_{SUB}$  of random particles and replace their masses according to the power-law in Equation (2).

### 3.2. The baryonic component of UMi

The spatial stellar density profiles of elliptical systems are commonly described as a power law in radius

$$\rho_*(r) = \frac{(3 - \gamma)M_*}{4\pi} \frac{a}{r^\gamma(r+a)^{\beta-\gamma}}, \quad (3)$$

where  $M_*$  is the total stellar mass and  $a$  is the scale radius. For  $\beta = 4$ , these models have simple analytic properties and are called Dehnen models (Dehnen 1993; Tremaine et al. 1994). In these models the densities are proportional to  $r^{-4}$  at large radii and diverge in the center as  $r^{-\gamma}$ . To model the bulk stellar component in UMi we used a Dehnen model (Dehnen 1993) where  $\gamma = 3/2$ . This slope most closely resembles the de Vaucouleurs model in surface density. We took the scale radius for the underlying stellar component in the UMi galaxy to be  $a = 0.4$  kpc (Kleyna et al. 1998; Palma et al. 2003). We set the total mass of the stellar component to be  $M_* = 9 \times 10^5 M_\odot$  taking the typical value of the mass-to-light ratio  $\Upsilon_* = 3$ .

We performed an  $N$ -body simulation with the DM halo and the underlying stellar components together. The resulting system was found to be stationary for a Hubble time (i.e. the density profile of the stellar component and the velocity dispersion stayed approximately constant for a Hubble time). The stellar velocity dispersion ( $\sigma \sim 10$  km s $^{-1}$ ) was in agreement with the velocity dispersion of the stellar component found in UMi ( $\sigma = 9.3, 12, 9.5 \pm 1.2$  km s $^{-1}$ ; Wilkinson et al. 2004; Gilmore et al. 2007; Walker et al. 2009).

Finally, for the initial density profile of the stellar clump, we take

$$\rho_c(r) = \rho_0 \exp(-r^2/2r_c^2), \quad (4)$$

with the clump radius  $r_c$  between 12 pc and 35 pc (Palma et al. 2003). The clump’s velocity dispersion was set to 1 km s $^{-1}$ . The clump was dropped at a galactocentric distance of 0.39 kpc in a circular orbit in the  $(x, y)$  plane (see also Sánchez-Salcedo & Lora 2010). Since the clump’s stars have the same color as the underlying stellar population in UMi (Kleyna et al. 1998), we assume that the  $V$ -band mass-to-light ratio  $M/L_V$  of the clump is the same as it is for the underlying stellar component (say,  $\Upsilon_* = 3$ ). Thus, the mass of the clump  $M_c$  is  $\simeq 4 \times 10^4 M_\odot$ .

### 3.3. The code

Since the internal two-body relaxation timescales for the three components (clump, underlying stellar component and halo) are much larger than one Hubble time, this system can be represented as collisionless (Binney & Tremaine 2008). We simulated the evolution of the UMi dwarf galaxy (stellar clump, underlying stellar component and DM halo) using the  $N$ -body code SUPERBOX (Fellhauer et al. 2000). SUPERBOX is a highly efficient particle-mesh, collisionless-dynamics code with high resolution sub-grids. The parameters of each model are given in Table 1.

In our case, SUPERBOX uses three nested grids centered in the center of density of the UMi dSph galaxy. We used  $128^3$  cubic cells for each of the grids. The inner grid is meant to resolve the inner region of UMi and the outer

grid (with a radii of 1000 kpc for all cases) resolves the stars that are stripped away from UMi’s potential. The spatial resolution is determined by the number of grid cells per dimension ( $N_c$ ) and the grid radius ( $r_{\text{grid}}$ ). Then the side length of one grid cell is defined as  $l = \frac{2r_{\text{grid}}}{N_c - 4}$ . To study the convergence of the results with different resolutions, we performed three simulations: a simulation with  $128^3$  cubic cells, one with higher ( $256^3$  cubic cells) and one with lower ( $64^3$  cubic cells) resolution of model *M3* (see model parameters in Table 1). We obtained practically the same results for the three resolutions. We conclude that  $128^3$  cubic cells suffices to achieve a robust accuracy. For  $N_c = 128$ , the resolution, which is of the order of the typical distance between the particles in the simulation, is given at the two last columns of Table 2.

*SUPERBOX* integrates the equations of motion with a leap-frog algorithm, and a constant time step  $dt$ . We selected a time step of  $dt = 0.1$  Myr in our simulations in order to guarantee that the energy (for the isolated components) is conserved better than 1%. The properties of the three modeled components of UMi (DM halo, underlying stellar component and stellar clump) used in the simulation are shown in Table 2. Also, the radii of the inner, middle and outer grids for each of the components are given.

#### 4. RESULTS

Our  $N$ -body simulations were carried out from a time  $t = 0$  to  $t = 10$  Gyr using the code described in Section 3.3. In Table 1 we list the parameters used in the simulations (see also §3.2). For the models *M1* – *M4* (small-core halo) we used  $10^6$  particles to represent the halo component,  $10^5$  particles for the bulk stellar component, and  $10^4$  particles for the stellar clump. For the models *M5* – *M8* (big core halo) we used the same particle number mentioned before for the underlying stellar component and for the stellar clump, but we used  $1.5 \times 10^7$  particles for the halo component. This was done in order to have the same mass per particle in both small ( $2 \times 10^9 M_\odot$ ) and big ( $3 \times 10^{10} M_\odot$ ) core DM halos. In total we have a set of 8 simulations (see *M1*–*M8* in Table 1).

##### 4.1. Halo without substructure

In Figure 1 we show the evolution of the clump in the models *M1* (clump radius  $r_c = 12$  pc) and *M3* (clump radius  $r_c = 35$  pc) for a halo with a small core ( $r_s = 0.91$  kpc). At  $t = 1$  Gyr in model *M1*, the clump inflated its radius by a factor  $\sim 1.5$  due to gravitational encounters with the halo particles, but it preserves its identity (see panel (b) of Figure 1). In model *M3*, the clump appears to be very disrupted already at  $t = 1$  Gyr (see panel (e) in Figure 1). We can say that, regardless the clump radius, the clump is totally destroyed at  $t = 2.5$  Gyr in both models (see panels (c) and (f) in Figure 1).

In order to quantify the destruction time of UMi’s stellar clump in our simulations, we built a map of the surface density of the stellar clump in the  $(x, y)$ -plane at any given time  $t$  in the simulation. We sample this two-dimensional map searching for the  $10 \times 10$  pc size parcel that contains the highest mass (number of clump particles). This region will be centered at the remnant of

the clump. We define that a clump is destroyed when this region has reached a density of  $1M_\odot \text{ pc}^{-2}$ . When such a small value of the surface mass density is reached by UMi’s clump, the column density of the clump is so low that it would be unrecognisable from the underlying stellar component, and would be thus undetectable.

Figure 2 shows the surface density of mass as a function of time, where the black line represents the surface density at which the clump is disrupted. The destruction times for both clumps in the small-core case are 1.8 and 0.9 Gyr for  $r_c = 12$  pc and  $r_c = 35$  pc, respectively (see last column of Table 1). This implies that a halo core of  $\sim 0.4$  kpc is not large enough to guarantee the survival of the clump. This result is in agreement with Kleyna et al.’s (2003) statement that if the core radius of the DM halo is equal to or smaller than the clump’s orbit, the clump will get destroyed within  $\sim 2$  Gyr. We recall that, in this case, the DM halo has a core radius of  $\sim 0.4$  kpc and the clump has a galactocentric distance of 0.39 kpc.

In Figure 3 we show the evolution of the clump for both  $r_c = 12$  pc (*M5*) and  $r_c = 35$  pc (*M7*), embedded in a halo with a large core ( $r_s = 2.2$  kpc). In both cases the clump survives for  $\sim$  Hubble time. The small ( $r_c = 12$  pc) clump expands up to  $\sim 2$  times of its original size in the first 5 Gyr (see panel (b) of Figure 3). After that, it maintains this size over one Hubble time. In the *M7* model ( $r_c = 35$  pc), the clump loses some particles (see panel (e) of Figure 3) and slightly reduces its initial size (see panel (e) of Figure 3). Then the clump continues losing some particles and, as a consequence, it shrinks its initial size by a factor of  $\sim 2.5$  by the end of the simulation ( $\sim$  Hubble time), but remains undestroyed. The survival of the clump can also be seen in Figure 2; the surface mass densities in the *M5* and *M7* models lie well above the clump’s destruction line (indicated by the horizontal black line).

This set of simulations tells us that a halo with a large core allows the survival of both clumps for  $\sim$  Hubble time. This result reaffirms the belief that the UMi dSph galaxy should have a large core DM halo (Kleyna et al. 2003), instead of a cuspy DM density profile.

##### 4.2. Halo with substructure

In this section we present the same simulations as those in §4.1 but including substructure in the DM halo with  $f = 0.1$ ,  $M_{\text{max}} = 10^7 M_\odot$  and  $M_{\text{min}} = 10^{3.3} M_\odot$  (which is the maximum mass resolution for the DM halo particles). For the halo with a small core (where the total mass of UMi is  $M = 2 \times 10^9 M_\odot$ ), the number of substructure particles is of  $N_{\text{sub}} = 5836$ . For the halo with a large core ( $M = 3 \times 10^{10} M_\odot$ ), we require  $N_{\text{sub}} = 22483$ .

In Figure 4 we show snapshots of the models *M2* and *M4* (small-core clumpy DM halo) at  $t = 0, 1$  and 2.5 Gyr. The purple circles represent the DM particles, the small light gray circles represent UMi’s extended stellar component particles, the black points represent the particles that make up the stellar clump and in green we show the substructure particles. From Figure 4 (see panels *a*, *b* and *c*), we can see that the small ( $r_c = 12$  pc) clump has increased its size by a factor of  $\sim 2$  after 1 Gyr, slightly larger compared to the case without substructure. We built a map of the surface density of the stars initially in the clump (see Figure 5), similar as that in the case

without substructure. A clump with an initial radius of  $r_c = 35$  pc survives  $\sim 1$  Gyr, which is also approximately the same time as in the non-substructured case (see last column of Table 1). These results imply that the dissolution by tidal forces in a DM halo with a small core plays a major role in the dynamical evolution of the clump, more than the interaction between the massive substructure particles and the particles of the clump.

In Figure 6 we show the number of substructure particles with masses  $> 10^4 M_\odot$  inside a sphere of 0.39-kpc radius for models *M2* and *M4*. This radius corresponds to the radius at which the clump is orbiting, and thus massive subhalos within that radius will have a major effect in the clump’s destruction. In these models, the number of particles more massive than  $10^4 M_\odot$ , inside the clump’s orbit, ranges from 1 to 9, with a mean number of 5 particles.

In Figure 7 we show snapshots for the clumpy halo with a big core (models *M6* and *M8*) at  $t = 0, 0.5$  and  $1.5$  Gyr. In both simulations, the clump appears to be enlarged at  $t = 0.5$  Gyr (see panels *b* and *e* of Figure 7) and, at  $t = 1.5$  Gyr, it is practically disrupted. The clump is dissolved at 1.6 Gyr in model *M6*, and at 1.4 Gyr in model *M8*. The number of substructure particles with mass larger than  $10^4 M_\odot$  is shown in Figure 8. In the case of a halo with a big core, the number of particles with masses  $> 10^4 M_\odot$  inside a 0.39 kpc sphere ranges between 8 and 23, with a mean number of 16. In the models with a large core, but without substructure, the clumps (12 and 35 pc) remain undestroyed for  $\sim$  Hubble time, which means that the destruction of the clump in the clumpy halo case is due to the random walk in momentum space that the stars in the clump undergo by the collisions with the substructure particles. This effect is so important that even with a core as large as  $\sim 1$  kpc, the clump does not manage to survive the continuous encounters with the massive substructure particles of the DM halo.

#### 4.3. A comparison with analytical estimates

Sánchez-Salcedo & Lora (2007) studied the abundance of Very Massive Objects (VMO) in the DM halo of Fornax and UMi. These VMOs can be compared with the subhalos that we have studied in this paper for UMi. In the impulse approximation, they found that, if the progenitor cluster became unbound immediately after formation, the mass of the VMOs should be

$$M_h \leq 2.5 \times 10^3 M_\odot \left( \frac{f \rho_{\text{dm}}}{0.1 M_\odot \text{ pc}^{-3}} \right)^{-1} \left( \frac{\sigma_{\text{dm}}}{20 \text{ km s}^{-1}} \right) \quad (5)$$

in order to have a clump as dynamically cold as observed. Here  $\rho_{\text{dm}}$  and  $\sigma_{\text{dm}}$  are the density and velocity dispersion of the dark matter particles in the UMi halo. For  $f = 0.1$ , this upper limit implies  $M_h \leq 2.5 \times 10^4 M_\odot$ . Therefore, the maximum number of VMO within the orbital radius  $r_{\text{orb}}$  is  $\simeq 4\pi f r_{\text{orb}}^3 \rho_{\text{dm}} / (3M_h) \simeq 100$ . In the case of a mass spectrum, the maximum number of subhalos with masses  $\leq 2.5 \times 10^4 M_\odot$  are expected to be smaller because the dissolution time of the clump due to collisions with subhalos of mass  $M$  goes as  $\propto M^2 dN(M)$ .

Our  $N$ -body simulations have shown that, if the subhalos follow a mass spectrum and if self-gravity of the clump is taken into account,  $\sim 16$  subhalos with masses larger than  $10^4 M_\odot$  are enough to disrupt the clump if the tidal perturbation by the dark halo is also included.

## 5. CONCLUDING REMARKS

We studied the dynamical consequences of the putative substructure in UMi’s DM halo in the stellar component. We ran  $N$ -body simulations of a stellar clump orbiting in a live cored DM halo. If the distribution of mass in the dark halo is smooth, a dark halo with a scale length of 0.91 kpc, which corresponds to a core of  $\sim 0.4$  kpc, cannot preserve the integrity of the clump. On the other hand, for a dark halo with a big core (scale length of 2.2 kpc, core radius of  $\sim 1$  kpc), the clump survives for approximately a Hubble time (Kleyna et al. 2003).

When 10% of the original DM halo total mass resides in compact subhalos, the clump dissolves in roughly the same timescale in the small core case. This means that the dissolution effects by tidal forces by the small-core DM halo are greater than due to the gravitational scattering with the massive substructure particles.

In the big-core case there is a large number of particles in substructure ( $N_{\text{sub}} = 22483$ ) with a mean number of 16 particles inside a sphere of radius 0.39 kpc (the radius of the orbit of the clump) with masses greater than  $10^4 M_\odot$  throughout the simulation. The effect of the substructures over the clump in this case results in the complete destruction of the clump within  $\sim 1.6$  Gyr for the clump with  $r_c = 12$  pc and within  $\sim 1.4$  Gyr for the clump with  $r_c = 35$  pc. In a smooth dark-matter halo, the large DM core halo ensures the longevity of the clump for almost one Hubble time, but in a clumpy halo, the clump is erased because of the random walk in momentum space that the stars in the clump undergo by collisions with the massive substructure particles.

It remains to study a more realistic scenario where the subhalos are not point particles (in which case resembles more the case of VMOs) but are extended perturbers. It would be worthwhile to quantify the effect that these extended subhalos would imprint compared to the point mass case studied here, and see in a more general case if subhalos in dSph galaxies impose a strong test to the  $\Lambda$ CDM scenario. Preliminary simulations suggest that the disruption timescale of the clump increases by 60%–70% if subhalos are extended, which is not enough to account for the survival of the clump. A thorough study will be presented elsewhere.

V.L. gratefully acknowledges support from the Alexander von Humboldt Foundation fellowship, and the anonymous referee for very useful comments that improved the presentation of the paper.. A.J. and E.K.G. acknowledge support from the Collaborative Research Center “The Milky Way System” (SFB881) of the German Research Foundation (DFG), especially subprojects A1 and A2. F.J.S.S. was partly supported by CONACyT project 165584 and PAPIIT project IN106212.

## REFERENCES

- Avila-Reese, V., Colín, P., Valenzuela, O., D'Onghia, E., & Firmani, C. 2001, *ApJ*, 559, 516
- Battaglia, G., Helmi, A., Tolstoy, E., Irwin, M., Hill, V. & Jablonka, P., 2008, *ApJ*, 681, L13
- Benson, A. J., Frenk, C. S., Lacey, C. G., Baugh C. M., & Cole S. 2002, *MNRAS*, 333, 177
- Binney J. & Tremaine S. 2008, *Galactic Dynamics*, 2nd edn. Princeton Univ. Press, Princeton, NJ
- Bovill, M. S. & Ricotti, M., 2011, *ApJ*, 741, 18
- Boylan-Kolchin, M., Bullock, J. S. & Kaplinghat, M., 2011, *MNRAS*, 415, 40
- Carlberg, R. G. 2009, *ApJ*, 705, L223
- Carlberg R. G., et al., 2011, *ApJ*, 731, 124
- Carrera, R., Aparicio, A., Martínez-Delgado, D., Alonso-García, J., 2002, *AJ*, 123, 3199
- Cen, R. 2001, *ApJ*, 546, L77
- Chen, D. & McGaugh, S. 2010, *RAA*, 10, Issue 12, 1215
- de Blok, W. J. G., McGaugh, S. S., Bosma, A., & Rubin, V. C. 2001, *ApJ*, 552, L23
- Dehnen, W. 1993, *MNRAS*, 265, 250
- Diemand, J., Kuhlen, M., Madau, P., Zemp, M., Moore, B., Potter, D., & Stadel, J. 2008, *Nature*, 454, 735
- El-Zant, A., Shlosman, I., & Hoffman, Y. 2001, *ApJ*, 560, 636
- Fellhauer, M., Kroupa, P., Baumgardt, H., Bien, R., Boily, C. M., Spurzem, R. & Wassmer, N., 2000, *New Astron.*, 5, 305
- Font, A. S. et al. 2011, *MNRAS*, 417, 1260
- Gao L., White S. D. M., Jenkins A., Stoehr F., Springel V., 2004, *MNRAS*, 355, 819
- Gilmore, G., Wilkinson, M. I., Wyse, R. F. G., Kleyana, J. T., Koch, A. et al. 2007, *AJ*, 663, 94
- GoerdT, T., Moore, B., Read, J. I., Stadel, J. & Zemp, M., 2006, *MNRAS*, 368, 1073
- GoerdT, T., Moore, B., Read, J. I., Stadel, J. & Zemp, M., 2010, *ApJ*, 725, 1707
- Governato, F. et al. 2010, *Nature*, 463, 203
- Governato, F. et al. 2012, *MNRAS*, 422, 1231
- Grebel, E. K., Gallagher, J. S., & Harbeck, D., 2003, *AJ*, 125, 1924
- Green, A. M., Hofmann, S., & Schwarz, D. J., 2005, *JCAP*, 08, 003
- Hofmann, S., Schwarz, D. J., & Stöcker, H. 2001, *Phys. Rev. D*, 64, 083507
- Jardel, J. R., & Gebhardt, K. 2012, *ApJ*, 746, 89
- Jin, S., Ostriker, J. P., & Wilkinson, M. I. 2005, *MNRAS*, 359, 104
- Johnston, K. V., Spergel, D. N., & Haydn, C. 2002, *ApJ*, 570, 656
- Kannan, R., Maccio, A. V., Pasquali, A., Moster, B. P. & Walter, F. 2012, *ApJ*, 746, 10
- Kaplinghat, M., Knox, L., & Turner, M. S. 2000, *Physical Review Lett.*, 85, 3335
- Khoperskov, A. V., Just, A., Korchagin, V. I., Jalali, M. A., 2007, *A&A*, 473, 31
- Kleyana, J. T., Geller, M. J., Kenyon, S. J., Kutz, M. J., Thorstensen, J. R., 1998, *ApJ*, 115, 2359
- Kleyana, J. T., Wilkinson, M. I., Gilmore, G. & Evans, N. W., 2003, *ApJ*, 588, L21
- Klypin, A., Kravtsov, A., Valenzuela, O. & Prada, F., 1999, *ApJ*, 522, 82
- Kniazev, A. Y., Brosch, N., Hoffman, G. L., Grebel, E. K., Zucker, D. B. & Pustilnik, S. A. 2009, *MNRAS*, 400, 2054
- Lora, V., Sánchez-Salcedo, F. J., Raga, A. C. & Esquivel, A., 2009, *ApJ*, 699, L113
- Ma, C.-P., & Boylan-Kolchin, M. 2004, *Phys. Rev. Lett.*, 93, 021301
- Macciò, A. V., Stinson, G., Brook, C. B., Wadsley, J., Couchman, H. M. P., Shen, S., Gibson, B. K., & Quinn, T. 2012, *ApJ*, 744, L9
- Mashchenko, S., Couchman, H. M. P., & Wadsley, J. 2006, *Nature*, 442, 539
- Mateo, M. L., 1998, *ARA&A*, 36, 435
- Mo, H. J., & Mao, S. 2004, *MNRAS*, 353, 829
- Moore, B., Ghigna, S., Governato, F., Lake, G., Quinn, T., Stadel, J., & Tozzi, P. 1999, *ApJ*, 524, L19
- Navarro J. F., Frenk C. S. & White S. D. M., 1996, *ApJ*, 462, 563
- Odenkirchen, M., Grebel, E. K., Harbeck, D., Dehnen, W., Rix, H. W., et al. 2001, *AJ*, 122, 2538
- Ostriker, J. P. & Steinhardt, P., 2003, *Science*, 300, 1909
- Palma, C., Majewski, S. R., Siegel, M. H., Patterson, R. J., Ostheimer, J. C. & Link, R., 2003, *AJ*, 125, 1352
- Peñarrubia, J., Kroupa, S. E., Walker, M. G., Gilmore, G., Wyn E. N. & Mackay, C. D. 2010, [arXiv:1005.5388]
- Peñarrubia, J., Navarro, J. F. & McConnachie, A. W., 2008, *ApJ*, 673, 266
- Pontzen, A., & Governato, F. 2012, *MNRAS*, 421, 3464
- Read, J. I., Wilkinson, M. I., Evans, N. W., Gilmore, G., Kleyana, J. T., 2006, *MNRAS*, 367, 387
- Rocha, M., Peter, A. H. G., Bullock, J. S., 2011, arXiv:1110.0464
- Romano-Díaz, E., Shlosman, I., Heller, C. & Hoffman, Y., 2008, *ApJ*, 687, L13
- Romano-Díaz, E., Shlosman, I., Heller, C. & Hoffman, Y., 2009, *ApJ*, 702, 1250
- Sánchez-Salcedo, F. J. 2003, *ApJ*, 591, L107
- Sánchez-Salcedo, F. J., Reyes-Iturbide, J. & Hernandez, X., 2006, *MNRAS*, 370, 1829.
- Sánchez-Salcedo, F. J., & Lora, V., 2007, *ApJ*, 658, L83
- Sánchez-Salcedo, F. J., & Lora, V., 2010, *MNRAS*, 407, 1135
- Somerville, R. S. 2002, *ApJ*, 572, 23
- Shu, F. H., Adams, F. C., Lizano, S., 1987, *ARA&A*, 25, 23
- Spergel, D. N., & Steinhardt, P. J. 2000, *Physical Review Lett.*, 84, 3760
- Springel, V., Wang, J., Vogelsberger, M., Ludlow, A., Jenkins, A., Helmi, A., Navarro, J. F., Frenk, C. S. & White, S. D. M., 2008, *MNRAS*, 391, 1685
- Strigari, L. E., Bullock, J. S., Kaplinghat, M., Diemand, J., Kuhlen, K & Madau, P., 2007, *ApJ*, 669, 676
- Strigari, L. E., Bullock, J. S., Kaplinghat, M., Simon, J. D., Geha, M., Willman, B. & Walker, M. G., 2008, *Nature*, 454, 1096
- Totani, T. 2010, *PASJ*, 62, L1
- Tremaine, S., Richstone, D. O., Byun, Y.I., et al. 1994, *AJ*, 107, 634
- Walker, M. G., Mateo, M., Olszewski, E. W., Peñarrubia, J., Wyn E. N. & Gilmore, G. 2009, *ApJ*, 704, 1274
- Walker, M. G., & Peñarrubia, J. 2011, *ApJ*, 742, 20
- Widrow, L. M. 2000, *ApJS*, 131, 39
- Wilkinson, M. I., Kleyana, J. T., Evans, N. W., Gilmore, G. F., Irwin, M. J. & Grebel, E. K., 2004, *ApJ*, 611, L21
- Yoon, J. H., Johnston, K. V., & Hogg, D. W. 2011, *ApJ*, 731, 58
- Young, L. M., 2000, *AJ*, 117, 1758
- Young, L. M., 2000, *AJ*, 119, 188

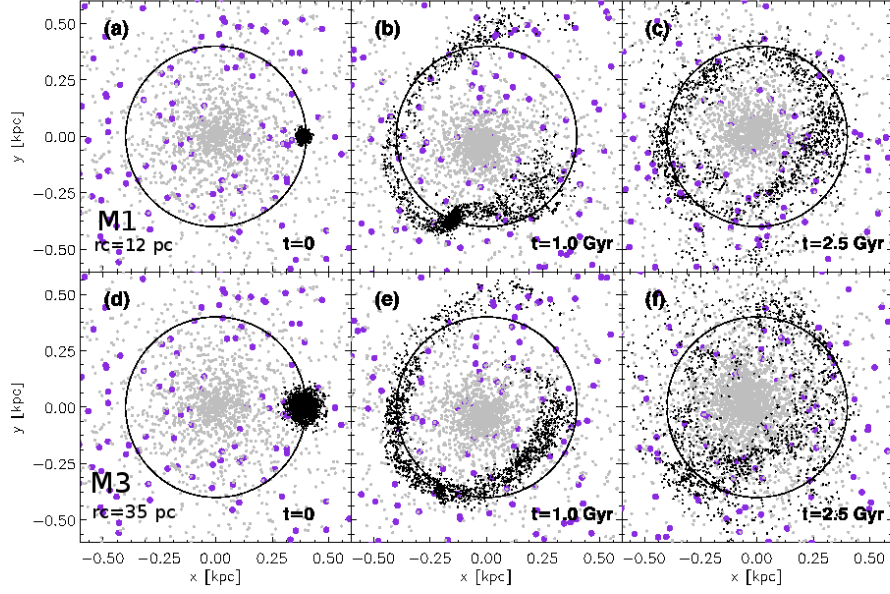


FIG. 1.— Evolution of a clump embedded in a smooth halo with a small core. The time is given at the bottom right corner. The top panels (a, b and c) show the case where the radius of the clump is  $r_c = 12$  pc (model M1). The bottom panels (d, e and f) show the case where the radius of the clump is  $r_c = 35$  pc (model M3). The purple circles represent the soft halo DM particles; the small light gray circles indicate the extended stellar component; and the black dots are for the particles of the stellar clump.

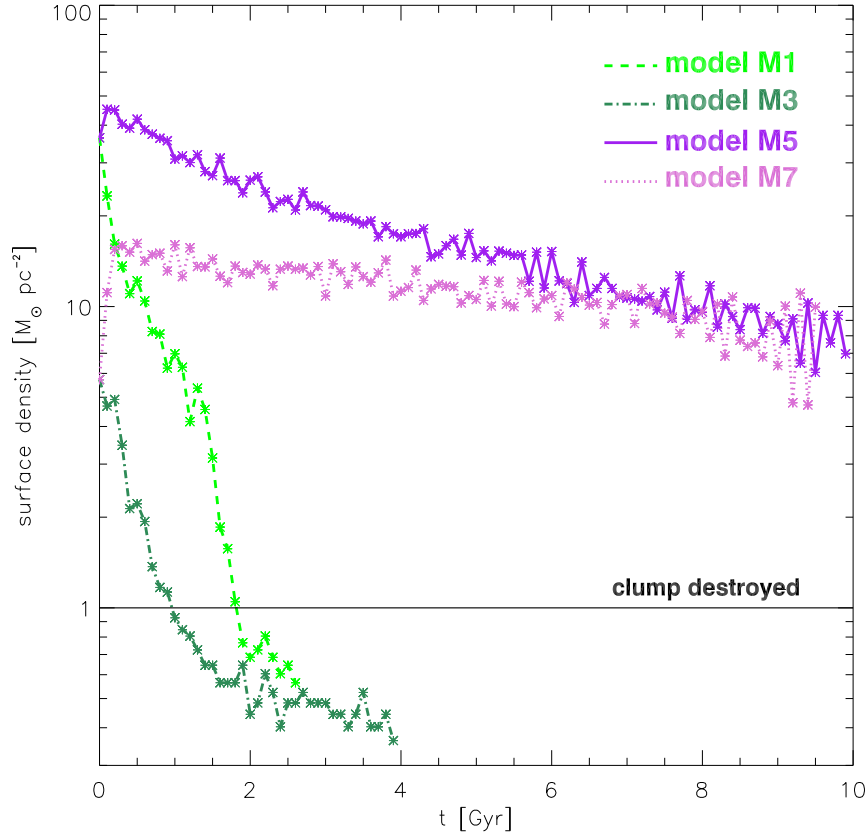


FIG. 2.— Surface density of the mass of UMi's clump map in the  $(x, y)$ -plane at any given time  $t$  in the simulation for the four models without substructure (see the models M1, M3, M5 and M7 in Table 1). The black line shows the destruction ( $1M_{\odot} \text{ pc}^{-2}$ ) line.

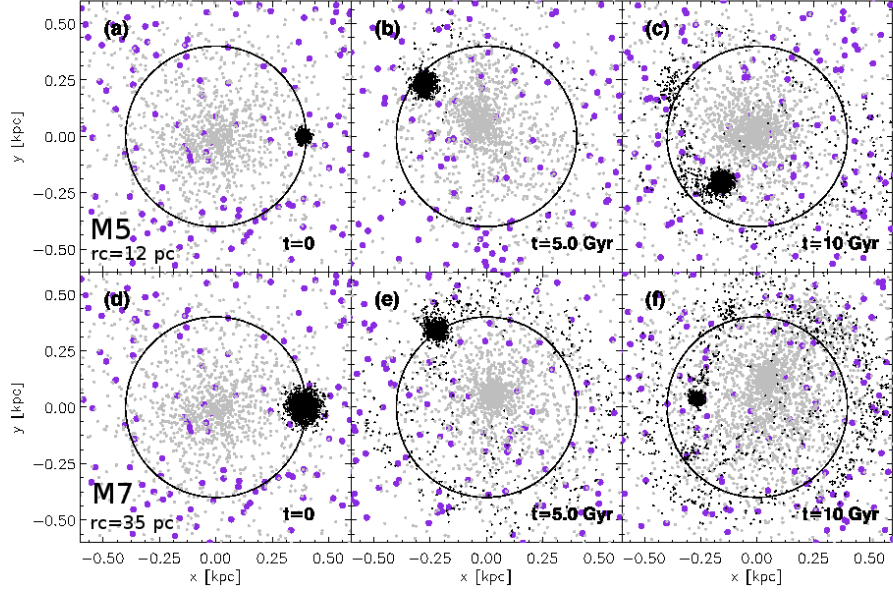


FIG. 3.— Same as Figure 1 but for the big-core DM halo and integration times  $t = 0, 5$  and 10 Gyr. The top panels show model  $M5$  and the bottom panels show model  $M7$ .

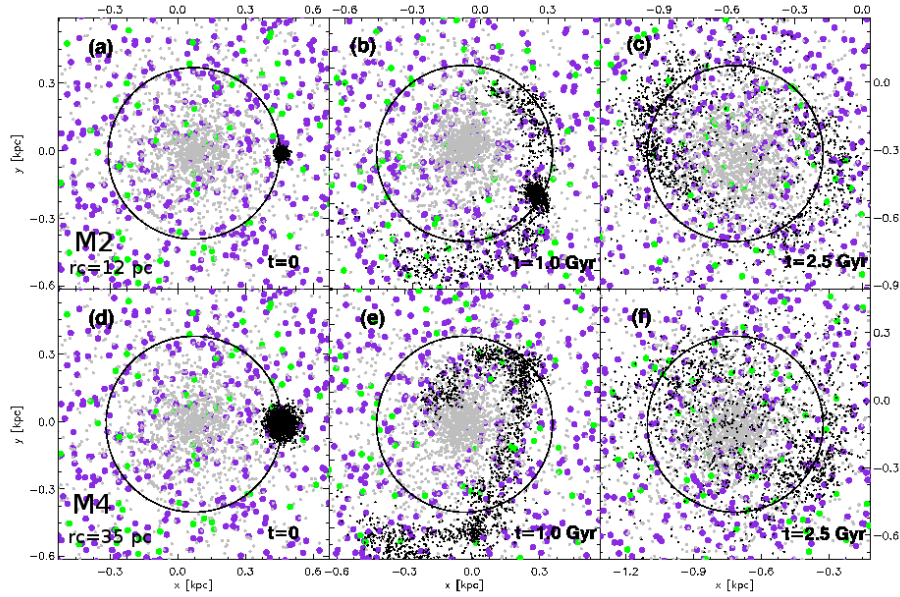


FIG. 4.— Snapshots at  $t = 0, 1$  and 2.5 Gyr for the small-core DM halo with 10% of the DM halo's total mass in substructure (green circles). The top panels show model  $M2$  and the bottom panels show model  $M4$ . The color code of the particles is the same as in Figure 1.



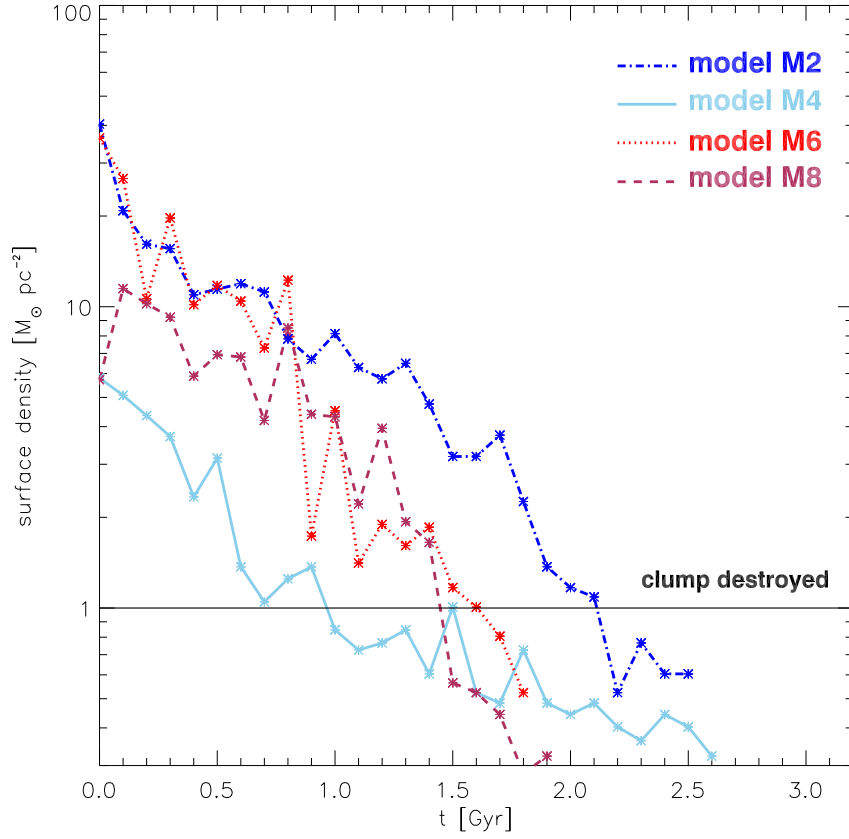


FIG. 5.— Same as Figure 2 for the four models with dark-matter subhalos (see models *M2*, *M4*, *M6* and *M8* in Table 1)

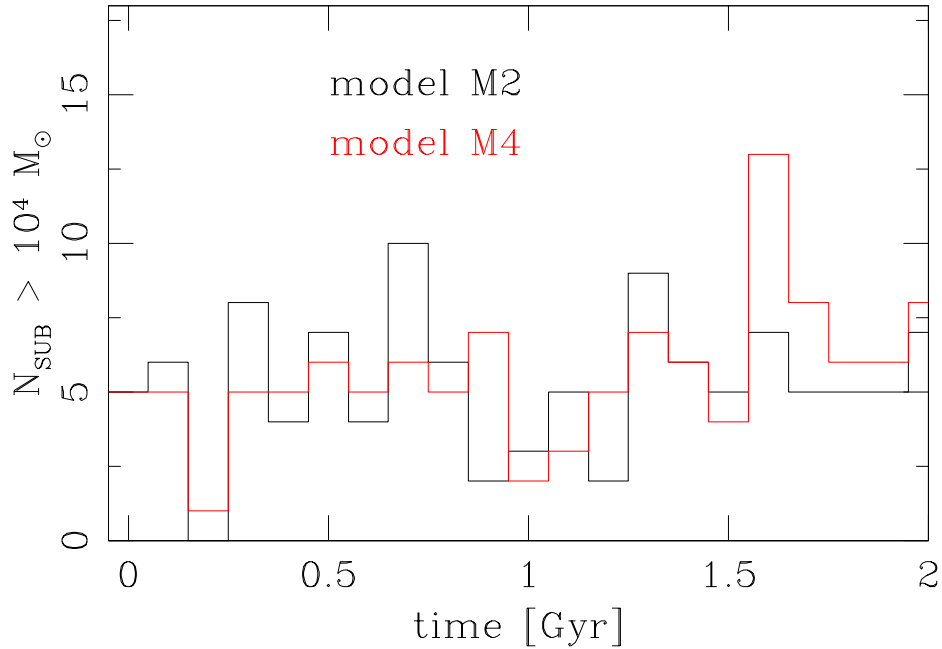


FIG. 6.— Number of halo particles with mass  $> 10^4 M_\odot$ , inside a 0.39 kpc sphere around the center of density of the simulation (i.e. inside the clump's orbit) for model *M2* (black line) for model *M4* (red line). The number of particles was computed at each 0.1 Gyr.

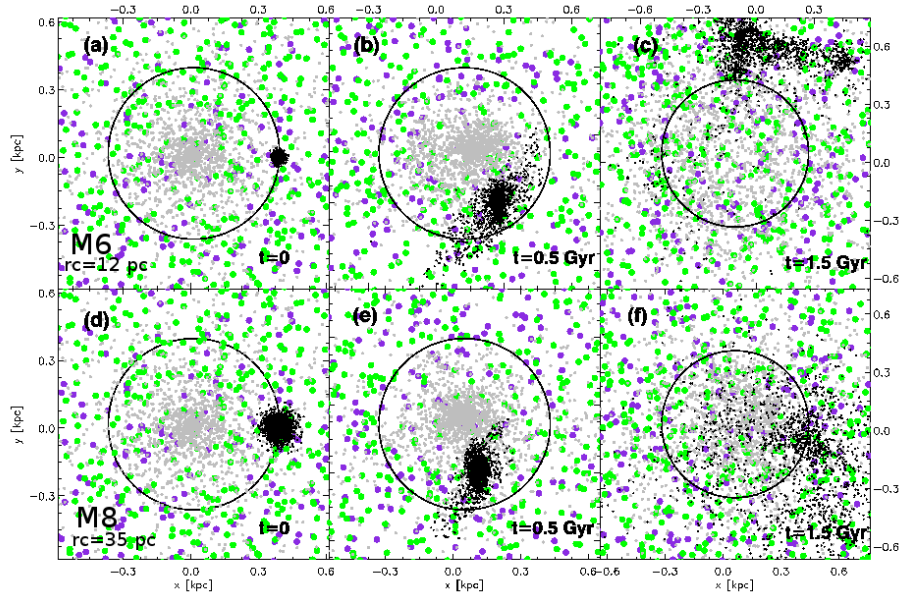


FIG. 7.— Same as Figure 4 but at times  $t = 0, 0.5$  and  $1.5$  Gyr. The top panels show model  $M6$  and the bottom panels show model  $M8$ .

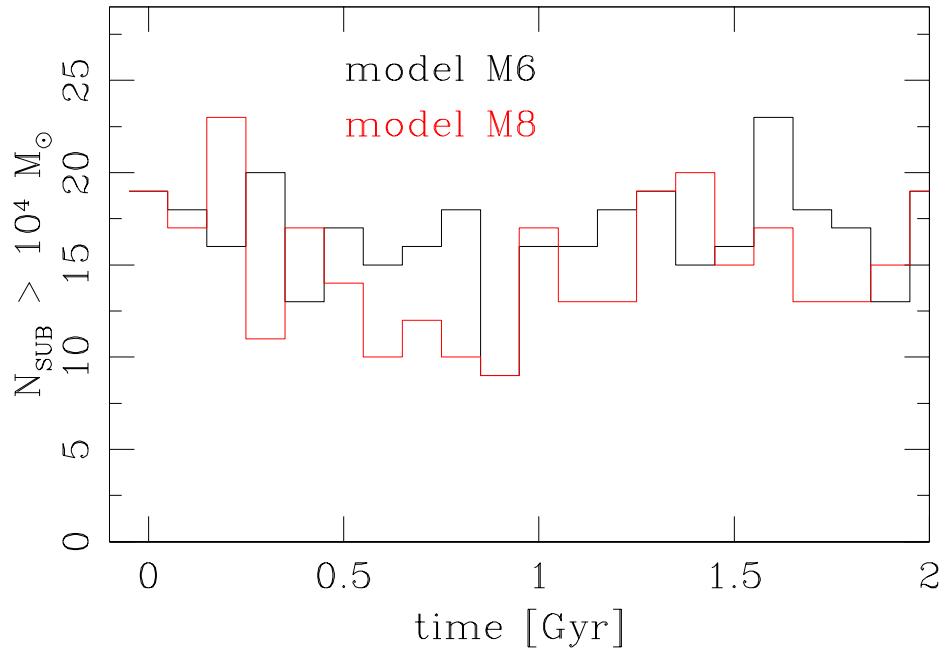


FIG. 8.— Same as Figure 6 but for models  $M6$  (black) and  $M8$  (red).

TABLE 1

PARAMETERS USED IN THE SIMULATIONS. HERE  $r_s$  ACCOUNTS FOR THE DM HALO SCALE LENGTH; M IS THE TOTAL MASS OF THE HALO, AND  $r_c$  IS THE RADIUS OF THE STELLAR CLUMP IN UMI.

Model	sub- structure	$r_s$ [kpc]	M [ $M_\odot$ ]	$r_c$ [pc]	destruction time [Gyr]
M1	no	0.91	$2 \times 10^9$	12	$\sim 1.8$
M2	yes	0.91	$2 \times 10^9$	12	$\sim 2.1$
M3	no	0.91	$2 \times 10^9$	35	$\sim 0.9$
M4	yes	0.91	$2 \times 10^9$	35	$\sim 1$
M5	no	2.2	$3 \times 10^{10}$	12	$> 10$
M6	yes	2.2	$3 \times 10^{10}$	12	$\sim 1.6$
M7	no	2.2	$3 \times 10^{10}$	35	$> 10$
M8	yes	2.2	$3 \times 10^{10}$	35	$\sim 1.4$

TABLE 2

SETUP PROPERTIES OF THE PARTICLES IN THE SIMULATIONS. TOTAL MASS, MASS PER PARTICLE AND NUMBER OF PARTICLES OF THE THREE UMi MODELED COMPONENTS, THE RADII OF THE GRIDS AND THE RESOLUTION  $l$  OF THE MIDDLE GRID (FOR  $N_c = 128$ ) ARE SHOWN.

Component	M [ $M_\odot$ ]	$m_p$ [ $M_\odot$ ]	N $10^6$	inner grid [kpc]	middle grid [kpc]	$l_{128}$ [kpc]
Halo with small core	$2 \times 10^9$	$2 \times 10^3$	1	1	20	0.322
Halo with large core	$3 \times 10^{10}$	$2 \times 10^3$	15	2	30	0.483
Extended stellar component	$9 \times 10^5$	9	0.1	1	10	0.161
Clump with $r_c = 12$ pc	$4.03 \times 10^4$	4.03	0.01	0.012	0.12	0.0019
Clump with $r_c = 35$ pc	$4.03 \times 10^4$	4.03	0.01	0.035	0.35	0.0056